

NASA TECHNICAL NOTE



NASA TN D-3373

e.1

NASA TN D-3373

LOAN COPY: RETURN
AFWL (W11L-2)
KIRTLAND AFB, N M

0130547



TECH LIBRARY KAFB, NM

**EFFECT OF PROPELLANT INJECTION
VELOCITY ON SCREECH IN 20 000-POUND
HYDROGEN-OXYGEN ROCKET ENGINE**

*by John P. Wanbainen, Harold C. Parish, and E. William Conrad
Lewis Research Center
Cleveland, Ohio*



NASA TN D-3373

EFFECT OF PROPELLANT INJECTION VELOCITY ON SCREECH
IN 20 000-POUND HYDROGEN-OXYGEN ROCKET ENGINE

By John P. Wanhainen, Harold C. Parish, and E. William Conrad

Lewis Research Center
Cleveland, Ohio

NATIONAL AERONAUTICS AND SPACE ADMINISTRATION

For sale by the Clearinghouse for Federal Scientific and Technical Information
Springfield, Virginia 22151 - Price \$0.45

EFFECT OF PROPELLANT INJECTION VELOCITY ON SCREECH IN 20 000-POUND HYDROGEN-OXYGEN ROCKET ENGINE

by John P. Wanhainen, Harold C. Parish, and E. William Conrad

Lewis Research Center

SUMMARY

An investigation was conducted at the Lewis Research Center to determine the effect of changes in propellant injection areas on screech stability characteristics of a rocket engine. Thirteen concentric tube injectors were evaluated: nine configurations with conventional straight-bore oxidizer elements, two configurations with taper-reamed oxidizer elements, one configuration with counterbored oxidizer elements, and one configuration with recessed oxidizer elements. Stability data were obtained at a chamber pressure of 300 pounds per square inch absolute and over a range of oxidant-fuel ratios from 4 to 7. Hydrogen injection temperature was used to rate the stability of the various designs. The injector with the lowest self-triggering temperature was considered to be the most stable design.

The hydrogen temperature at which screech occurred could be reduced to less than 60° R (minimum available) by selection of hydrogen-to-oxygen injection area ratios of less than one. The combustion stability boundary correlated with hydrogen-to-oxygen injection velocity ratio irrespective of the hydrogen temperature level; at a velocity ratio above $6\frac{1}{2}$ combustion was stable and below $6\frac{1}{2}$, unstable. The stable operating limits of both the tapered and counterbored oxidizer element configurations correlated with data of conventional injectors when based on exit area ratio. Recessing the oxidizer tubes below the surface of the faceplate also improved the stability.

INTRODUCTION

Although numerous comprehensive investigations of high-frequency combustion instability have been conducted in both laboratory and full scale rocket engines, very little design information has been generated to assist in the development of future engines.

This situation arose because most of these efforts were aimed at either verifying theoretical models or developing fixes for specific engines.

Along with many other variables, the effect of propellant injection velocity on screech has not been systematically defined, although this is one of the easier variables to control. For the physical combustion model of reference 1, the injection velocity had an appreciable influence on stability characteristics of the combustor. The effort discussed herein was, therefore, undertaken to provide injector design information relative to velocity effects applicable to hydrogen-oxygen rocket engines. The experiments were conducted with concentric-tube-type injectors in 20 000-pound-thrust engines operating at a chamber pressure of 300 pounds per square inch. The contraction ratio of the combustor was 1.89. This engine size was chosen to allow reasonable flexibility and to minimize the cost, yet was large enough to allow confidence in the applicability of the test results.

Hydrogen injection temperature was used to rate the stability characteristics of the various injector designs. The rating criterion was based on unpublished data obtained at Lewis and results of the J-2 engine development program (J-2 engine quarterly progress reports) which indicated that hydrogen-oxygen combustion could be destabilized by reducing hydrogen injection temperature. A temperature ramping technique was developed that could reduce hydrogen inlet temperature in a typical run by as much as 25^o R per second. High-response carbon-resistor type probes in the injector cavity were used to determine the hydrogen temperature at which instability was encountered.

A range of both hydrogen and oxygen injection velocities was covered by reaming out the center oxygen tubes or altering the gap of the hydrogen annulus around the oxygen tubes. Oxygen velocity was varied from 25 to 120 feet per second. A range of hydrogen velocities from 100 to 1000 feet per second was covered. Hydrogen-to-oxygen velocity ratio varied from 1 to 40. The effects of taper-reamed and counterbored oxygen tubes, as well as recessed oxygen tubes, were also assessed.

APPARATUS

Test Facility

The Rocket Engine Test Facility of the Lewis Research Center is a 50 000-pound-thrust sea level stand equipped with an exhaust gas muffler and scrubber. A sketch of the facility is shown in figure 1. The engine was mounted on the thrust stand (fig. 2) to fire vertically into the scrubber where the exhaust gases were sprayed with water at rates to 50 000 gallons per minute for the purpose of cooling and sound suppression. The cooled exhaust gases were discharged into the atmosphere from the 70-foot exhaust

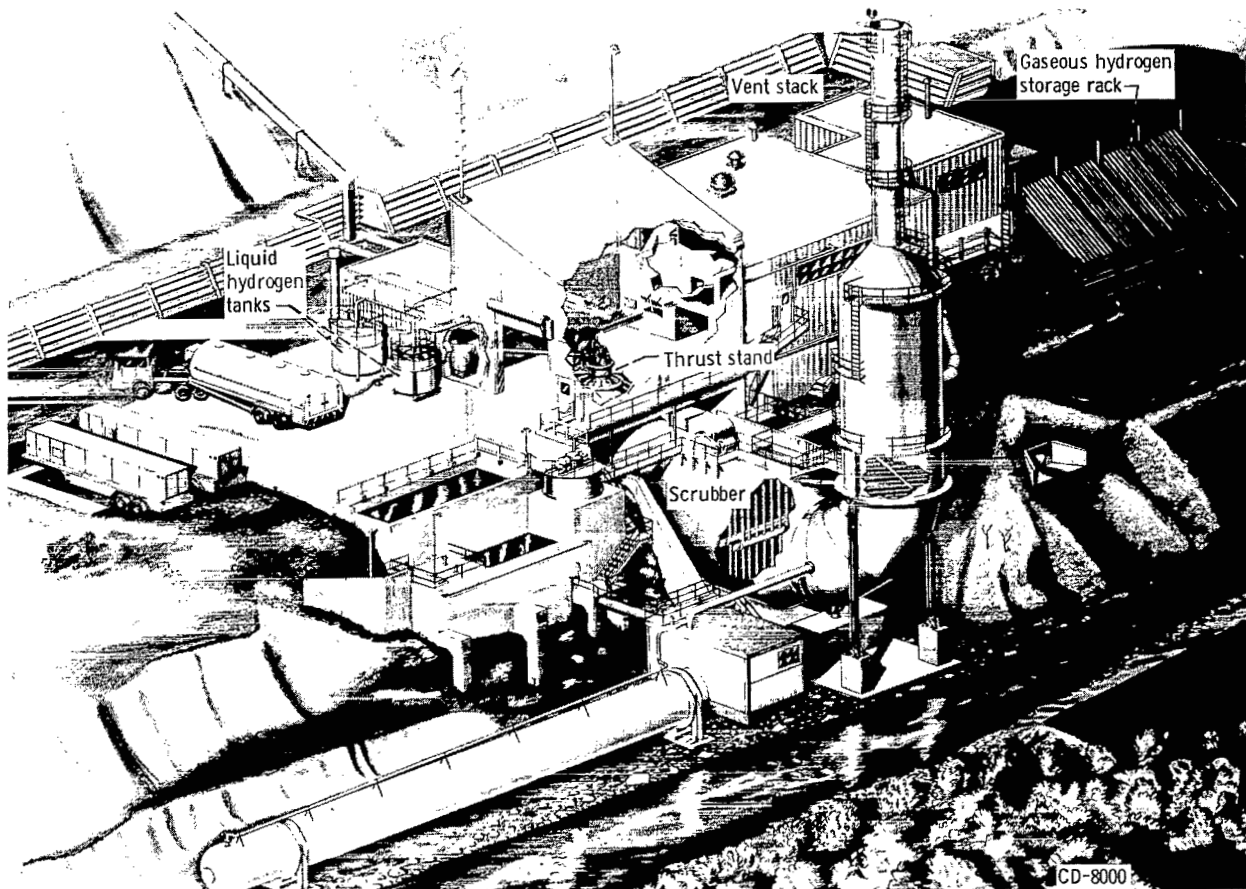


Figure 1. - Rocket engine test facility.

stack. Initially, carbon dioxide was used to make the scrubber inert before and after each run to prevent explosions. Later in the program, pilot flames were installed at various locations in the scrubber to burn excess hydrogen. These burnoff jets were completely successful and eliminated the need for the expensive and time-consuming carbon dioxide inerting operation.

The facility utilized a pressurized propellant system to deliver the propellants to the engine from the storage tanks. The oxygen propellant line was immersed in a nitrogen bath, and the liquid hydrogen line was insulated with a plastic-type foam. The propellant storage tanks consisted of 75-cubic-foot and 175-cubic-foot liquid hydrogen Dewars, a 120 000-standard-cubic-foot (2200 psi) gaseous hydrogen storage rack, and a 55-cubic-foot liquid oxygen tank submerged in a liquid nitrogen bath.

The facility was operated remotely from a control room located 2000 feet from the facility. In addition to a central data retrieval system, the facility was equipped with several direct reading oscillographs and tape recorders to record test results.

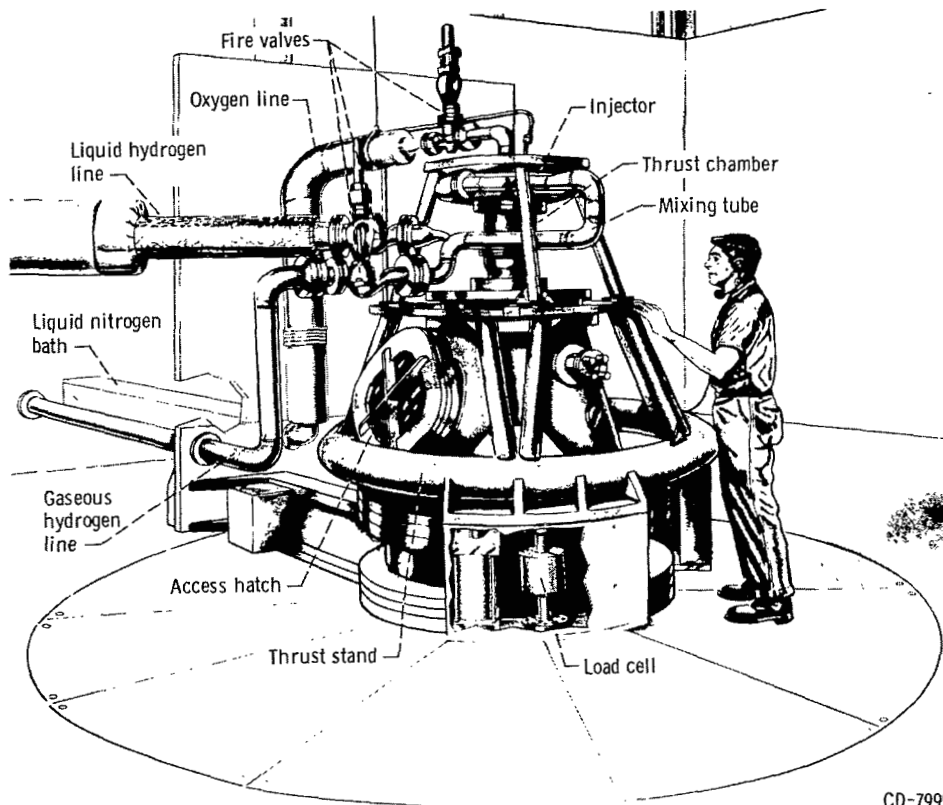


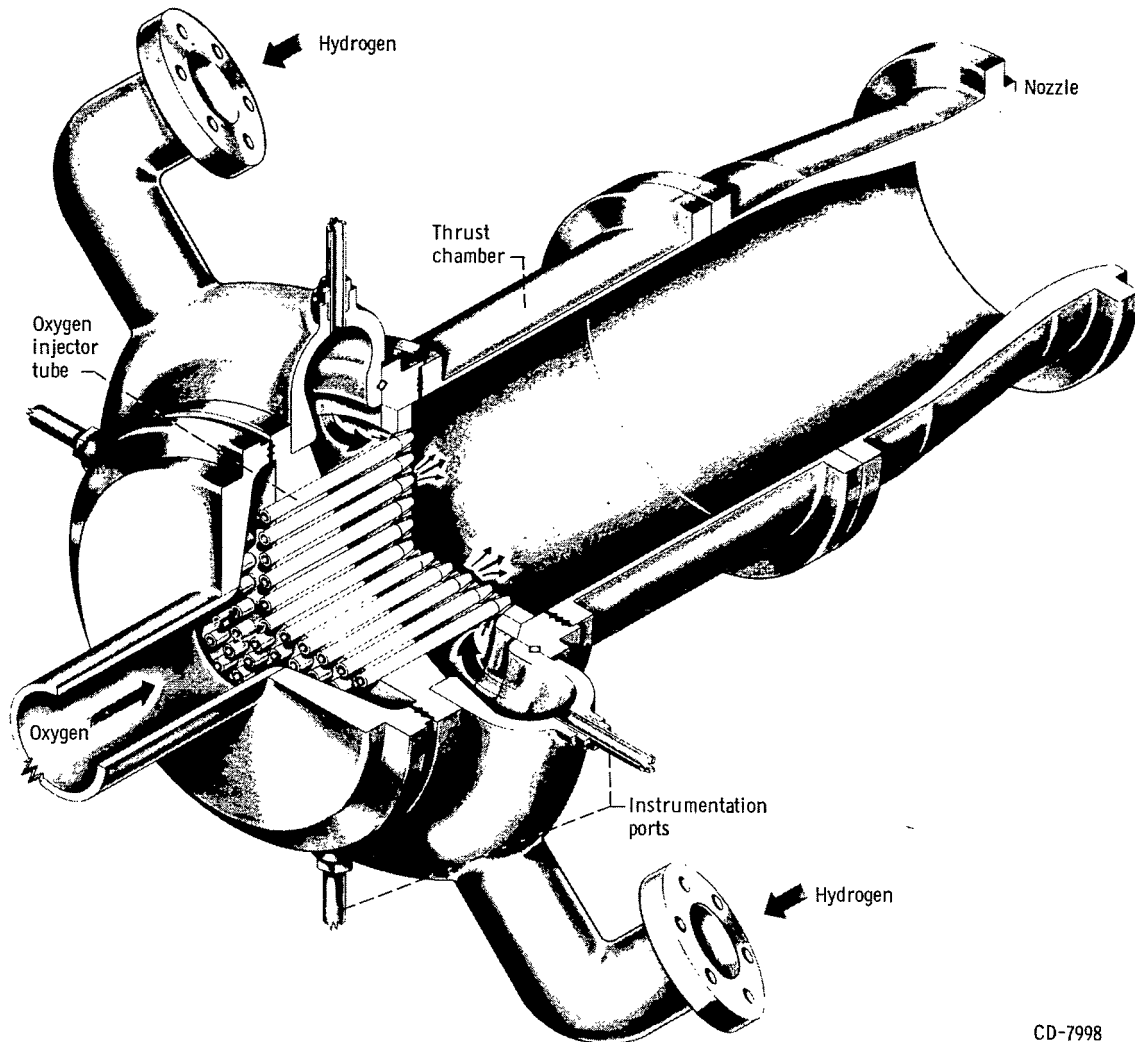
Figure 2. - Engine mounted on thrust stand.

Engine

The rocket combustor (fig. 3) was composed of an injector with removable faceplates, a cylindrical heat-sink thrust chamber with a 10.77-inch inside diameter and a convergent-divergent heat-sink exhaust nozzle with a contraction ratio of 1.89 and an expansion area ratio of 1.3. The inner surfaces of the mild steel heat-sink thrust chamber and nozzle were coated with 0.030-inch-thick flame-sprayed zirconium oxide to reduce the rate of heat transfer into the metal. This allowed a run duration of 3 seconds which was adequate to obtain the required data.

Injector

A faceplate and cross-sectional views of the 421-element concentric-tube injector are presented in figures 4 and 5, respectively. The faceplates were fabricated from 1/2-inch-thick copper, a material with a good heat-sink capability and good thermal con-



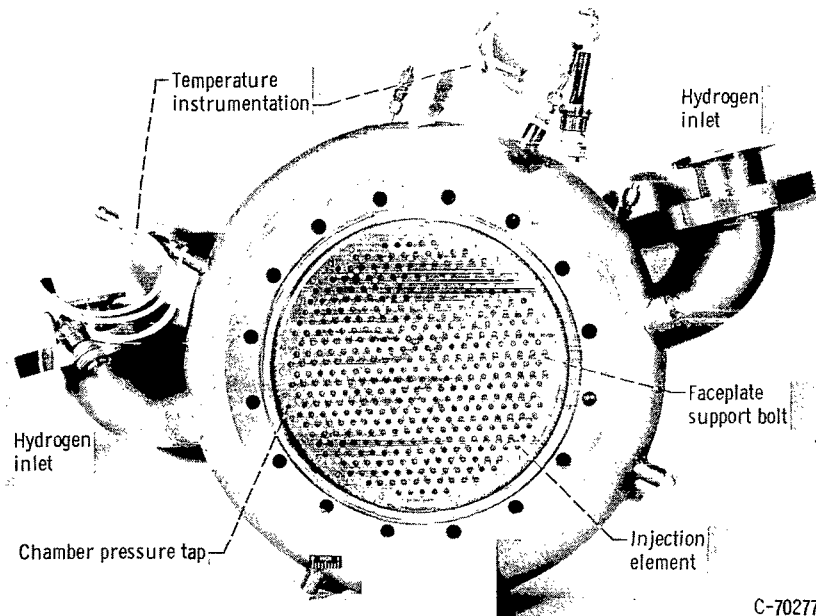
CD-7998

Figure 3. - Hydrogen-oxygen rocket engine.

ductivity; thus the injector cooling design was simplified. The impingement angle (half) of the hydrogen was 10° . The configurations investigated are identified with oxygen and hydrogen orifice diameters and injection areas in table I. The measurements were taken in the plane of the oxygen tube exit. Cross-sectional views of variations in oxygen tube exit geometries, which include a straight-bore element, a taper-reamed element, a counterbored element, and a recessed element are shown in figure 6.

Hydrogen Temperature Controller

The hydrogen temperature ramp was accomplished by starting the run on a mixture

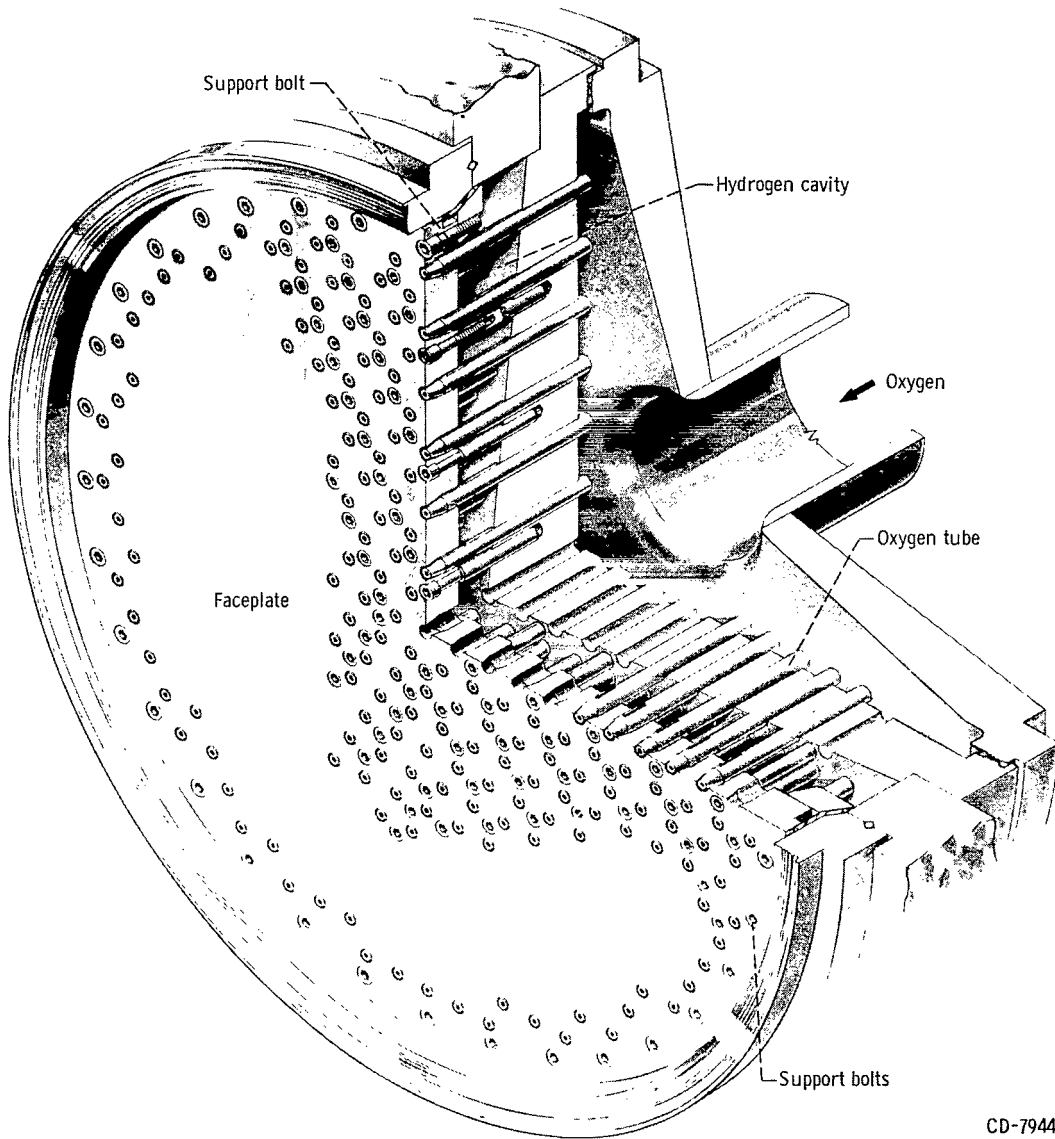


C-70277

Figure 4. - Concentric-tube injector. Faceplate diameter, 10.78.

TABLE I. - TEST CONFIGURATIONS

Configuration	Diameter of oxygen orifice, D_{O_2} , in.	Diameter of hydrogen orifice, D_{H_2} , in.	Oxygen injection area, A_{O_2} , in.	Hydrogen injection area, in. ²	Injection area ratio, A_{H_2}/A_{O_2}
Straight bore (see fig. 6(a)) ↓	0.052	0.134	0.894	0.771	0.862
	.052	.141	.894	1.41	1.58
	.052	.172	.894	4.62	5.17
	.0635	.172	1.33	4.62	3.47
	.0635	.204	1.33	8.58	6.45
	.081	.134	2.17	.771	.36
	.081	.141	2.17	1.41	.65
	.081	.172	2.17	4.62	2.13
	.081	.204	2.17	8.58	3.95
	.081	.172	2.17	4.62	2.13
	Taper (see fig. 6(b))	.110	.172	4.00	4.62
Taper (see fig. 6(c))	.110	.172	4.00	4.62	1.16
Counterbore (see fig. 6(d))	.052	.172	.894	4.84	5.41
Recess (see fig. 6(e))					



CD-7944

Figure 5. - Cross section of concentric-tube injector.

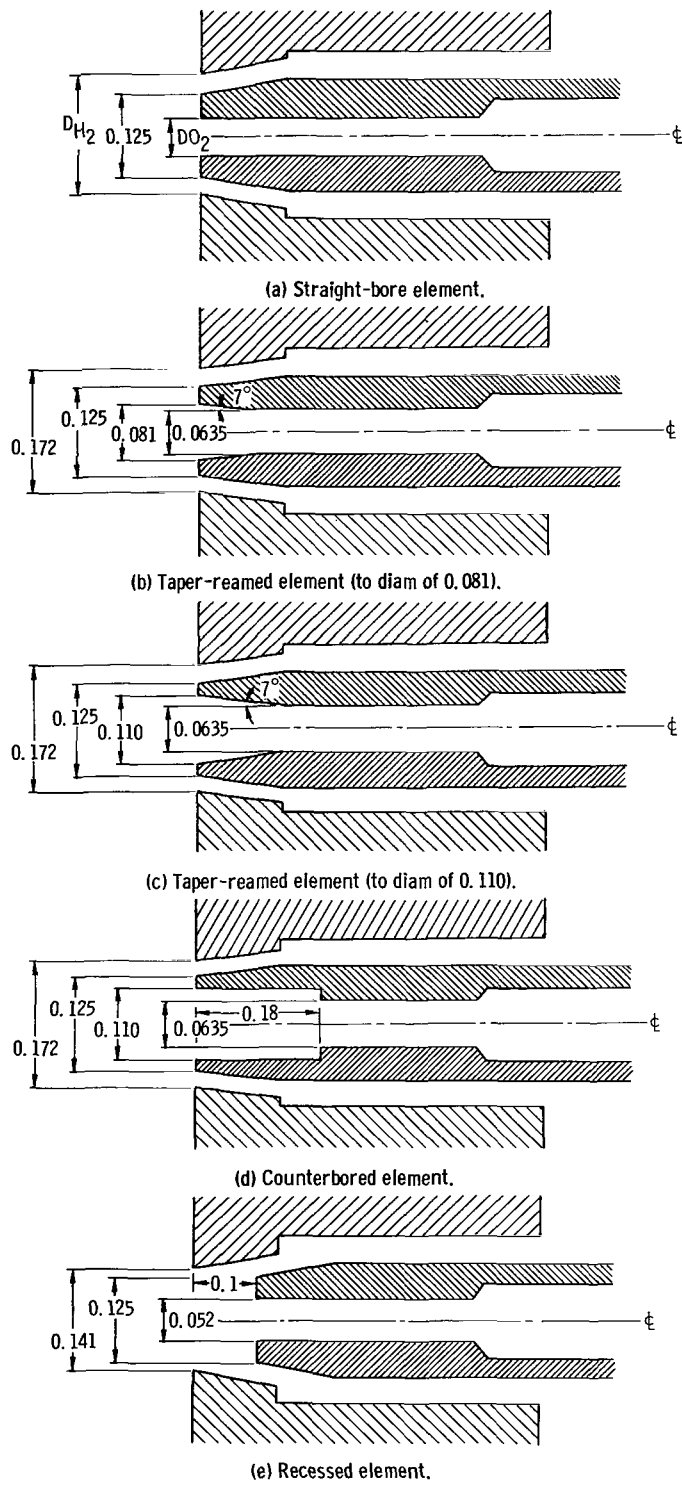
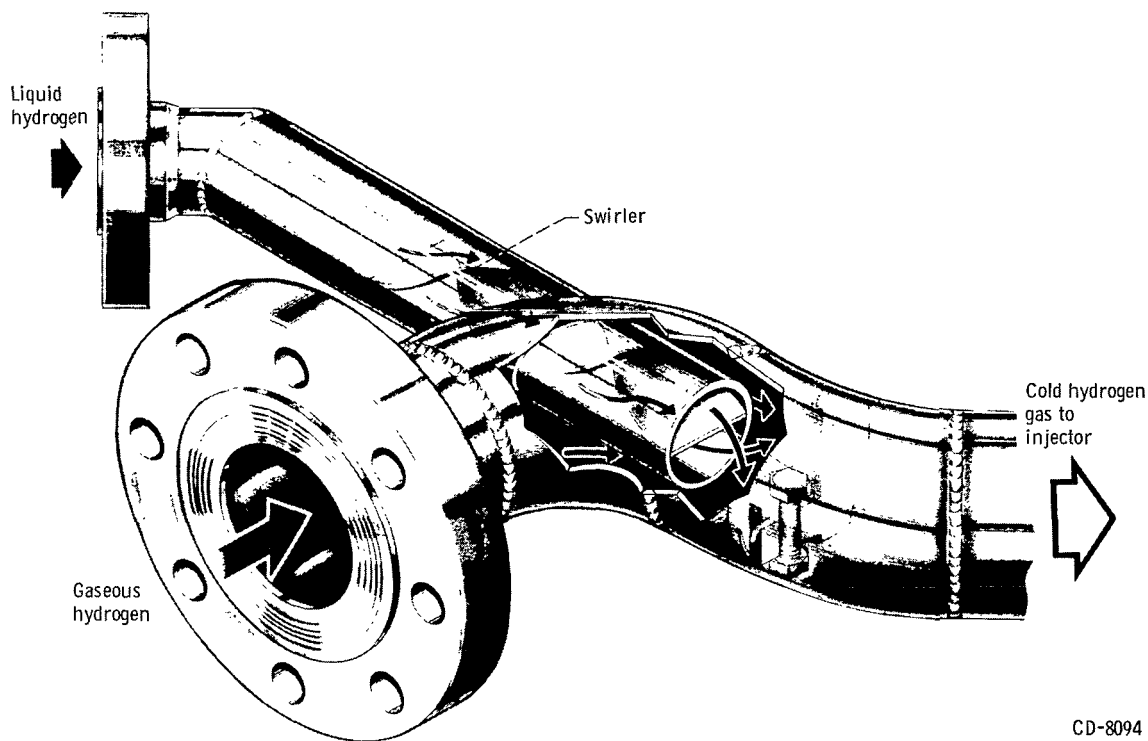


Figure 6. - Cross-sectional views of injector elements (all dimensions are in inches).



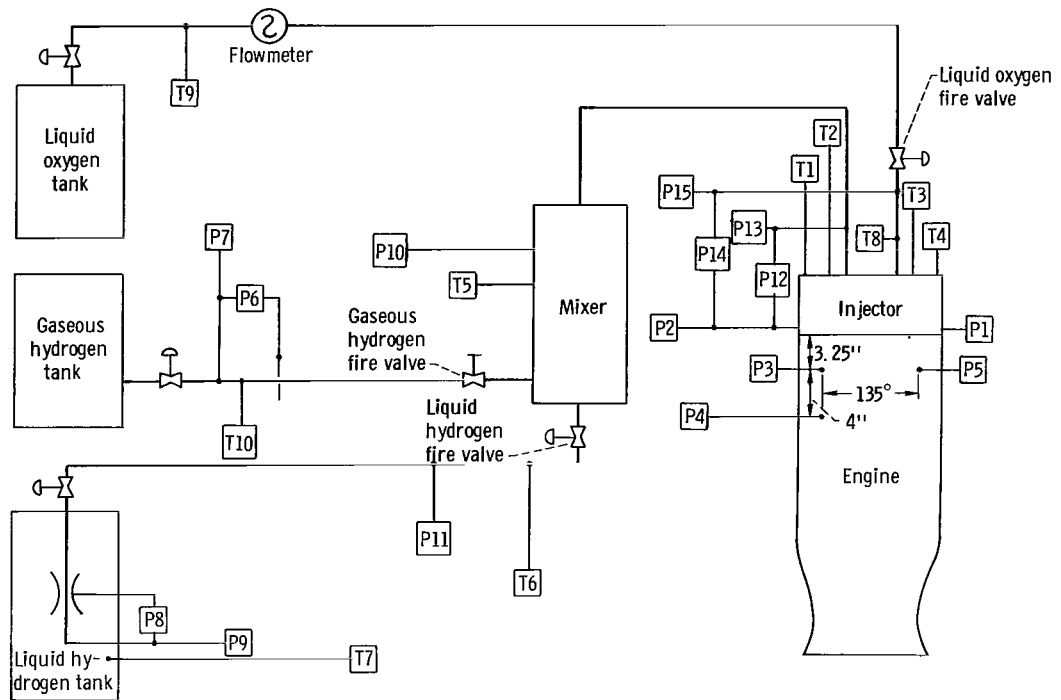
CD-8094

Figure 7. - Schematic of mixing station.

of liquid hydrogen and warm gaseous hydrogen and then reducing the percentage of gas introduced in a predetermined ramp while simultaneously opening the liquid hydrogen valve to maintain a constant total flow. Mixing was accomplished by swirling the liquid into the gaseous hydrogen stream. The mixing station was in a manifold outside the injector with an intervening volume of 1140 cubic inches. A schematic of the mixer is shown in figure 7. Flow rates of gaseous hydrogen and liquid hydrogen to the mixer were controlled with valves that were operated by an electrohydraulic servosystem.

Instrumentation

The instrumentation used in the investigation and the location of the various transducers are shown in figure 8. The signals from the transducers were transmitted to the Lewis Research Center automatic digital data recording system. Piezoelectric, water-cooled, flush-mounted pressure transducers were used at three locations on the thrust chamber to determine the character and phase relation of the pressure field and to allow identification of the screech mode. The response characteristics of the transducers were flat to within 10 percent to a frequency of 6000 cps and had a nominal resonant frequency of about 20 000 cps in the water-cooled mount. The signals from high-frequency



- | | | | |
|-----|---|-----|---|
| P1 | Static chamber pressure (injector face), four-arm strain gage transducer 1 | P14 | Oxygen injection differential pressure, four-arm strain gage transducer |
| P2 | Static chamber pressure (injector face), four-arm strain gage transducer 2 | P15 | Oxygen injection pressure, four-arm strain gage transducer |
| P3 | Dynamic chamber pressure, water-cooled quartz pressure transducer 3 | T1 | Hydrogen injector temperature, carbon resistor sensor probe 1 |
| P4 | Dynamic chamber pressure, water-cooled quartz pressure transducer 4 | T2 | Hydrogen injector temperature, carbon resistor sensor probe 2 |
| P5 | Dynamic chamber pressure, water-cooled quartz pressure transducer 5 | T3 | Hydrogen injector temperature, carbon resistor sensor probe 3 |
| P6 | Gaseous hydrogen orifice differential pressure, four-arm strain gage transducer | T4 | Hydrogen injector temperature, carbon resistor sensor probe 4 |
| P7 | Gaseous hydrogen orifice pressure, four-arm strain gage transducer | T5 | Hydrogen mixer temperature, carbon resistor sensor probe |
| P8 | Liquid hydrogen venturi differential pressure, four-arm strain gage type | T6 | Liquid hydrogen line temperature, carbon resistor sensor probe |
| P9 | Liquid hydrogen venturi pressure, four-arm strain gage transducer | T7 | Liquid hydrogen venturi temperature, platinum type |
| P10 | Hydrogen mixer pressure, four-arm strain gage transducer | T8 | Oxygen injection temperature, copper-constantan thermocouple |
| P11 | Liquid hydrogen line pressure, four-arm strain gage transducer | T9 | Oxygen flowmeter temperature, platinum type |
| P12 | Hydrogen injection differential pressure, four-arm strain gage transducer | T10 | Gaseous hydrogen orifice temperature, iron-constantan thermocouple |
| P13 | Hydrogen injection pressure, four-arm strain gage transducer | | |

Figure 8. - Instrumentation diagram.

response transducers were recorded in analog form on magnetic tape and were displayed on direct reading instruments for visual monitoring during the tests.

Oxygen propellant flow rate was determined with a vane flowmeter that was calibrated with water by using a static weighing system. The correction from water calibration to cryogenic calibration that accounted for the dimensional change of the instrument with temperature was obtained from the flowmeter manufacturer. Liquid hydrogen flow rate was measured by using a venturi, and the gaseous hydrogen flow rate was measured by using an orifice plate. The strain gage pressure transducers were calibrated by a commercial standard. Liquid flow temperatures were measured by platinum resistance sensors described in reference 2. The pressure and temperature systems were calibrated immediately before the data were acquired by an electrical two-step calibration system, which used resistances in an electrical circuit to simulate a given pressure. The maximum probable error in engine performance caused by measurement errors was determined to be approximately ± 2 percent.

PROCEDURE

As mentioned in the INTRODUCTION, the stability rating of each configuration was expressed in terms of the hydrogen temperature at which screech was encountered. The technique employed was to select an initial hydrogen temperature by presetting the valves of the mixer and by ramping the gas valve toward a closed position and the liquid valve toward an open position, about 1 second after ignition, to reduce the temperature of the injected hydrogen to a value below the anticipated screech limit. After the first transition point was obtained for a configuration, the ramp rate was reduced to minimize mass accumulation in the propellant system. The screech limit was obtained from high-speed recorder data wherein the injector hydrogen temperature in the injector cavity was read at the instant screech was indicated by an oscillograph trace of a flush-mounted pressure transducer. Combustion was considered unstable when a periodic wave-form with an amplitude substantially greater than the normal noise level was observed on the oscillograph record. A typical screech transition is presented in the RESULTS AND DISCUSSION section. Data were obtained over a range of oxidant-fuel ratios to establish a limit curve.

For those configurations that exhibited low screech temperatures, below about 70° R, it was necessary to prechill all hydrogen lines and valves down to the fire valve by a pre-flow and overboard venting of liquid nitrogen. In addition, still lower temperatures in the 55° to 65° R temperature range required the use of a 1-second lead of liquid hydrogen through the injector for prechill prior to stepping the mixer to the preset condition. Because of the use of heat-sink thrust chambers and nozzles it was necessary to limit run

TABLE II. - EXPERIMENTAL DATA

Test	Diameter of oxygen orifice, D_{O_2} , in.	Diameter of hydrogen orifice, D_{H_2} , in.	Hydrogen injection temperature, $^{\circ}R$	Static at pressure injector, P_{inj} , psia	Hydrogen weight flow, \dot{W}_{H_2} , lb/sec	Oxygen weight flow, \dot{W}_{O_2} , lb/sec	Oxidant-fuel ratio, O/F	Oxygen injector pressure drop, psi	Hydrogen injector pressure drop, psi	Oxygen injection velocity, V_{O_2} , ft/sec	Hydrogen injection velocity, V_{H_2} , ft/sec	Efficiency of characteristic exhaust velocity, η_{C^*} , percent	Location of element detail	Stability classification			
359	0.052	0.134	61.7	311.8	9.56	55.41	5.80	142.7	204.7	118.4	582	93.9	Fig. 6(a)	Stable			
360			64.3	314.7	9.12	55.35	6.07	152.2	249.6	118.3	638	96.5		Transition			
361			65.8	298.4	9.18	54.34	5.92	126.2	282.2	116.1	794	92.5		Stable			
362			61.6	296.3	10.25	48.71	4.75	112.4	248.8	104.1	632	94.9		Stable			
363			61.8	297.0	10.08	48.90	4.85	117.9	249.5	104.5	624	95.4		Stable			
364			65.4	273.0	8.58	53.05	6.18	122.5	227.7	113.4	916	88.1		Transition			
366			62.7	299.0	10.84	50.09	4.62	158.4	276.8	107.0	706	92.4		Stable			
367			66.1	314.9	10.01	50.60	5.06	132.5	284.2	108.1	831	99.4					
368			64.9	307.5	9.67	53.50	5.53	169.2	215.0	114.3	734	94.5					
369			64.7	308.6	8.28	53.75	6.49	167.5	226.2	114.9	616	99.9					
370			60.5	320.4	9.89	54.35	5.49	149.7	180.0	116.2	572	97.5					
371			61.1	325.7	9.09	57.60	6.34	177.5	100.6	123.1	532	98.4					
336			0.052	0.141	67.3	316.2	11.19	50.01	4.47	143.5	100.5	106.9		580	97.1	Fig. 6(a)	Transition
337	65.9	317.7			11.17	48.59	4.35	130.5	96.9	103.9	487	99.4					
339	71.8	314.2			10.16	50.35	4.96	137.6	115.2	107.6	752	99.1					
340	72.0	315.3			9.85	53.18	5.40	167.0	102.3	113.7	734	96.9					
341	72.7	306.6			9.34	54.62	5.85	176.5	108.8	116.8	757	94.4					
343	75.3	272.9			8.23	54.14	6.58	212.1	187.8	115.7	875	88.3	Stable				
344	67.5	299.6			10.57	45.63	4.32	119.4	82.2	97.5	624	99.7	Transition				
345	69.1	298.8			10.05	44.95	4.47	97.8	88.5	96.1	684	102.1					
346	68.2	300.1			9.30	49.75	5.35	143.4	82.5	106.3	590	98.1					
350	65.2	318.9			11.53	46.33	4.02	127.8	92.9	99.1	467	102.0					
351	65.4	294.8			11.82	46.16	3.91	212.6	78.2	98.7	556	94.1					
673	0.052	0.172			125.0	312.0	10.02	50.83	5.07	228.3	15.50	108.7	632	98.6	Fig. 6(a)		Transition
674					123.0	302.0	10.64	48.01	4.51	208.7	17.10	102.6	682	98.8			
675			155.0	313.0	9.22	54.41	5.90	234.3	21.64	116.3	744	97.5					
676			88.0	303.0	11.07	46.47	4.19	210.4	14.55	99.3	439	98.5					
148			132.0	320.6	11.60	50.70	4.37	-----	-----	108.4	760	96.7					
149			122.0	313.4	11.80	48.00	4.06	-----	-----	102.6	714	97.7					
151			135.0	324.7	10.50	55.00	5.24	-----	-----	117.6	700	95.4					
154			153.0	280.4	7.40	54.00	7.30	-----	-----	115.4	661	94.8					
155			154.0	277.3	7.45	52.50	7.05	-----	-----	112.2	675	95.1					
156			145.0	282.5	8.03	52.30	6.51	-----	-----	111.8	669	94.3					
157			129.0	296.9	9.25	51.80	5.60	-----	-----	110.7	639	94.8					
158			136.0	299.0	10.69	49.20	4.60	-----	-----	105.2	775	95.8					
159			139.0	283.0	9.52	51.40	5.39	-----	-----	109.9	750	89.9					
160	137.0	279.0	9.79	49.50	5.06	-----	-----	105.8	769	90.1							
161	129.0	278.0	10.03	47.20	4.71	-----	-----	100.9	737	91.9							
162	129.0	273.0	9.34	46.60	4.99	-----	-----	99.6	698	93.1							
405	0.0635	0.172	102.0	274.8	9.70	49.57	5.11	44.53	29.26	71.2	538	88.9	Fig. 6(a)	Transition			
407			87.0	264.8	10.49	45.75	4.36	60.13	33.02	65.8	474	88.7					
411			95.0	277.6	13.16	42.69	3.24	78.46	38.64	61.4	651	91.9					
412			116.0	301.3	8.67	54.20	6.25	80.10	27.83	79.9	519	95.8					
413			116.0	299.6	8.81	54.10	6.14	78.63	27.03	77.8	529	94.8					
414			108.0	294.3	7.84	53.35	6.80	77.30	21.80	76.7	435	98.1					
417	0.0635	0.204	153.0	311.1	9.87	52.32	5.30	73.31	20.15	75.2	428	95.9	Fig. 6(a)	Transition			
418			137.0	274.4	9.75	47.88	4.91	34.92	20.57	68.8	420	90.5		Unstable			
420			151.0	308.7	8.19	56.48	6.90	135.20	12.76	81.2	352	96.9		Unstable			
421			140.0	287.7	11.97	42.71	3.57	56.47	22.60	61.4	508	96.7		Transition			
424			154.0	306.8	9.38	52.52	5.60	75.30	20.65	75.5	416	95.9					
427			171.0	322.2	10.24	54.27	5.30	79.35	21.20	78.0	480	96.5					
428			193.0	320.5	9.96	53.67	5.39	69.29	16.65	77.0	505	97.6					

TABLE II. - Concluded. EXPERIMENTAL DATA

Test	Diameter of oxygen orifice, D_{O_2} , in.	Diameter of hydrogen orifice, D_{H_2} , in.	Hydrogen injection temperature, $^{\circ}R$	Static at pressure injector, P_{inj} , psia	Hydrogen weight flow, \dot{W}_{H_2} , lb/sec	Oxygen weight flow, \dot{W}_{O_2} , lb/sec	Oxidant-fuel ratio, O/F	Oxygen injector pressure drop, psi	Hydrogen injector pressure drop, psi	Oxygen injection velocity, V_{O_2} , ft/sec	Hydrogen injection velocity, V_{H_2} , ft/sec	Efficiency of characteristic exhaust velocity, η_{C^*} , percent	Location of element detail	Stability classification
373	0.081	0.134	64.1	290.3	8.36	51.35	6.14	34.69	309.6	45.2	627	96.7	Fig. 6(a)	Stable
374			59.3	285.1	9.13	47.95	5.25	35.31	310.4	42.2	522	96.2		
375			60.6	288.1	9.15	50.27	5.49	32.66	310.4	44.3	550	94.2		
376			66.4	296.3	9.07	50.48	5.57	42.70	311.2	44.5	869	97.2		
429	0.081	0.141	59.4	315.1	9.92	52.20	5.26	23.53	61.08	46.0	304	98.5	Fig. 6(a)	Stable
430			58.7	317.5	9.21	53.99	5.86	24.34	58.01	47.6	277	99.4		Stable
431			59.9	322.5	8.50	58.45	6.88	24.79	52.97	51.5	262	99.2		Stable
432			66.1	311.9	7.63	53.34	7.65	28.22	50.27	51.4	350	100.2		Transition
377	0.081	0.172	86.5	302.7	8.83	50.18	5.63	21.73	20.75	44.2	340	103.7	Fig. 6(a)	Transition
378			79.5	271.6	10.33	47.55	4.60	48.69	20.59	41.9	381	86.1		
379			72.5	293.3	11.97	42.62	3.56	13.74	20.33	37.5	313	99.2		
380			95.3	310.4	8.21	53.86	6.56	32.62	17.50	47.4	358	100.7		
381			104.0	321.3	8.54	55.89	6.54	31.01	18.14	49.2	411	100.6		
383			79.0	297.6	9.44	47.43	5.02	24.40	21.42	41.8	303	99.9		
384			90.7	282.6	7.03	54.12	7.70	-----	-----	47.7	316	97.3		
385			72.0	287.7	8.68	56.04	6.46	49.90	11.68	49.3	262.5	83.1		
389			72.0	298.4	9.96	48.55	4.87	9.60	15.53	42.8	248	96.8		
390			86.0	294.0	11.23	47.01	4.19	13.26	25.13	41.4	440	94.3		
391	0.081	0.204	117.0	311.1	9.96	50.87	5.09	9.76	14.52	44.6	312	98.6	Fig. 6(a)	Transition
392			101.0	296.2	10.38	47.15	4.54	9.58	13.88	41.5	281	97.0		
393			109.0	306.8	9.23	52.85	5.73	11.97	11.93	46.6	269	97.0		
397			90.5	275.2	11.32	47.23	4.17	18.53	7.01	41.6	281	87.9		
398			125.0	280.7	7.18	54.98	7.66	18.53	14.85	48.5	273	95.2		
400			125.0	311.5	8.81	55.03	6.25	15.25	13.54	48.6	300	97.6		
403			115.4	300.2	9.14	49.51	5.42	17.99	17.35	43.6	293	99.3		
404			132.0	305.8	7.46	58.15	7.80	17.37	12.43	51.2	277	98.8		
434	0.081	0.172	99.6	285.9	7.80	49.97	6.41	42.26	18.58	44.0	402	99.2	Fig. 6(b)	Transition
435			79.0	277.8	8.69	47.40	5.45	35.76	19.12	41.8	308	95.8		
436			101.0	301.4	7.63	55.33	7.25	53.91	19.74	48.7	378	99.0		
437			72.4	257.3	12.38	37.59	3.04	54.97	48.64	33.1	402	94.7		
438			73.6	285.3	11.96	46.30	3.87	42.84	21.20	40.8	345	90.7		Stable
439			74.3	290.2	10.29	46.01	4.47	36.43	18.76	40.5	297	96.7		Transition
440			72.3	290.3	10.26	47.20	4.60	40.99	18.58	41.6	273	95.0		Transition
442			85.0	298.3	8.66	54.41	6.28	50.96	16.48	47.9	327	94.3		Transition
470	0.110	0.172	66.3	293.1	10.57	49.32	4.66	6.08	18.50	23.5	176	90.7	Fig. 6(c)	Transition
471			69.6	291.0	9.93	49.66	5.00	34.91	15.13	23.7	223	91.7		
474			71.5	273.1	8.88	52.15	5.87	62.20	24.71	24.9	254	85.4		
475			72.0	267.7	8.35	53.39	6.39	48.23	19.32	25.5	246	85.5		
476			66.6	254.7	8.98	51.14	5.69	49.23	16.08	24.4	215	80.4		
493			59.4	306.8	11.87	47.01	3.96	45.56	8.71	22.4	112	96.7	Fig. 6(d)	Stable
494			63.5	282.9	9.79	49.73	5.08	47.06	9.57	23.7	119	90.5		Transition
495			78.2	303.4	8.46	56.32	6.65	60.54	18.12	26.9	256	94.7		
496			80.3	298.3	8.02	58.12	7.25	70.36	18.13	27.7	274	93.3		
497			86.9	290.0	8.04	57.02	7.09	68.27	19.10	27.2	333	91.8		
498			61.7	287.2	10.71	48.30	4.51	47.99	10.22	23.1	113	91.5		Stable
636	0.052	0.172	78.0	298.9	9.45	48.61	5.14	185.5	41.97	103.9	295	98.2	Fig. 6(e)	Transition
637			73.0	314.1	10.86	47.90	4.41	171.6	36.85	102.4	260	99.6		
638			97.0	312.1	9.23	54.39	5.89	216.4	52.99	116.4	408.1	96.1		
639			97.0	323.2	8.80	56.15	6.38	216.9	35.98	120.0	378	99.2		
640			77.0	310.8	9.68	49.24	5.08	189.6	36.28	105.3	433	100.5		

duration to 3 seconds; accordingly, all valve scheduling was accomplished by the use of an automatic sequence timer.

METHODS OF CALCULATION

The methods of calculation are covered in appendix B; however, one aspect is significant to the results to be presented and deserves consideration at this point. Determination of an accurate value of the instantaneous mass flow of hydrogen from the injector at the time of screech inception was difficult because of the use of the temperature-ramping technique. Because of a large change in hydrogen density with temperature, a significant amount of mass was accumulated during a temperature-ramp run between the flow measuring stations (liquid and gas) and the injector face. In the extreme case, hydrogen was stored in the system at a rate of about 2 pounds per second. Despite strenuous efforts to account for this source of error, the hydrogen injection velocities and oxidant-fuel ratios presented in the figures are undoubtedly subject to scatter and some error in mean value.

RESULTS AND DISCUSSION

In this investigation, hydrogen injection temperature was used to rate the screech stability characteristics of the various injector designs. The injector with the lowest self-triggering temperature was considered to be the most stable design. The results are presented in the following order:

- (1) Effect of Propellant Injection Area
- (2) Stability Correlation with Injection Velocities
- (3) Effect of Oxidant Tube Exit Geometry
- (4) Effect of Oxygen Tube Recess

The data were obtained with uniform-pattern, concentric-tube injectors with a thrust per element of approximately 48 pounds. Chamber pressure was nominally 300 pounds per square inch absolute for all tests. All data were obtained with the same thrust chamber geometry (contraction ratio of 1.89) to minimize changes in chamber and nozzle damping that could mask the effects of changes in injector configuration. In addition to a graphical presentation of the stability data, measured combustor parameters for each test such as chamber pressure, injector differential pressures, and propellant weight flows are listed in table II.

A typical oscillograph record of a test to determine the stable operating limits of a combustor in terms of hydrogen injection temperature is presented in figure 9. The

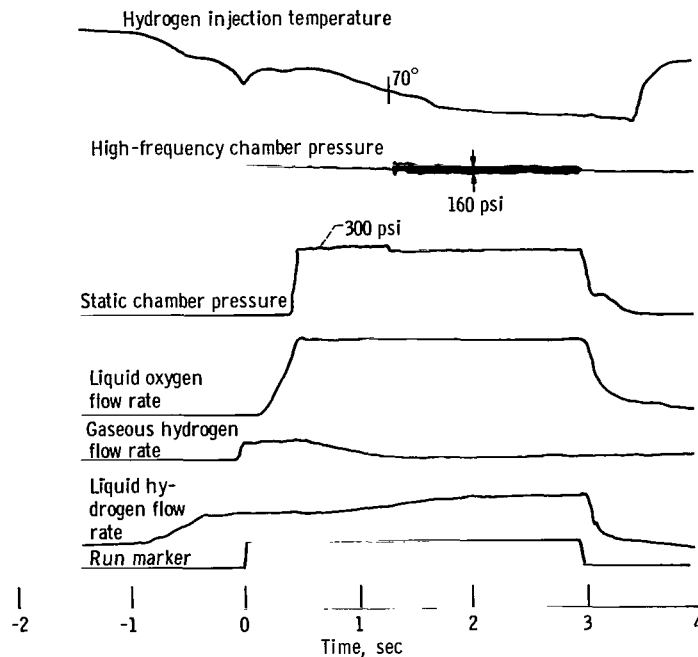


Figure 9. - Oscillograph traces of typical screech test illustrating the hydrogen temperature rating technique.

step change in the run marker is an indication that the solenoid that opens the oxygen fire valve has been energized. One second before the oxygen fire valve was opened a small amount of liquid hydrogen was allowed to flow through the propellant system and injector to reduce the metal temperature to a value close to the anticipated hydrogen transition temperature. Examination of the traces shows that after chamber pressure had reached rated conditions, the split of liquid hydrogen and gaseous hydrogen (ambient) flow was varied to lower the hydrogen injection temperature to encounter screech. Combustion instability was encountered at a temperature of 70° R in the example shown. The peak-to-peak amplitude of the chamber pressure oscillations that was measured by using a piezoelectric transducer flush mounted in the thrust chamber wall near the injector was about 160 pounds per square inch. The step change in the static chamber pressure trace, injector differential pressures, and injector manifold pressures (only the first parameter shown) at the time of transition from stable to unstable combustion was a typical occurrence. The variation in oxidant-fuel ratio during two typical temperature-ramp tests is shown in figure 10. The hydrogen temperature at the start of the tests was about 90° R and was then ramped through the transition point, which was approximately 70° R for the injector design. The time interval between data points is 0.032 second. A typical plot of pressure amplitude against frequency obtained from a spectrum analysis of chamber pressure during screech is presented in figure 11. The maximum pressure amplitude occurred at a frequency of about 3400 cycles per second, which closely cor-

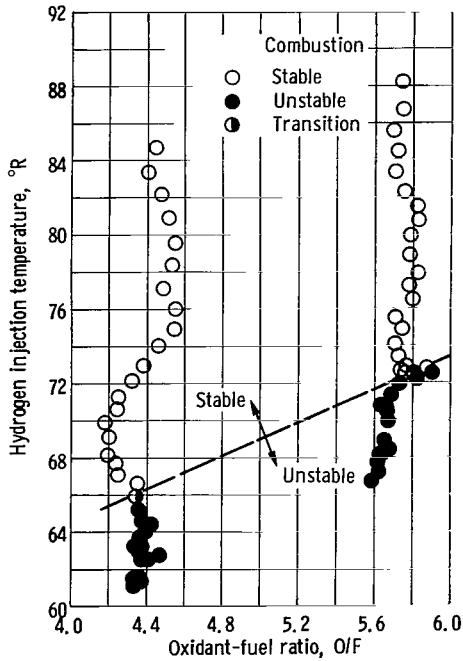


Figure 10. - Typical temperature-ramp tests.

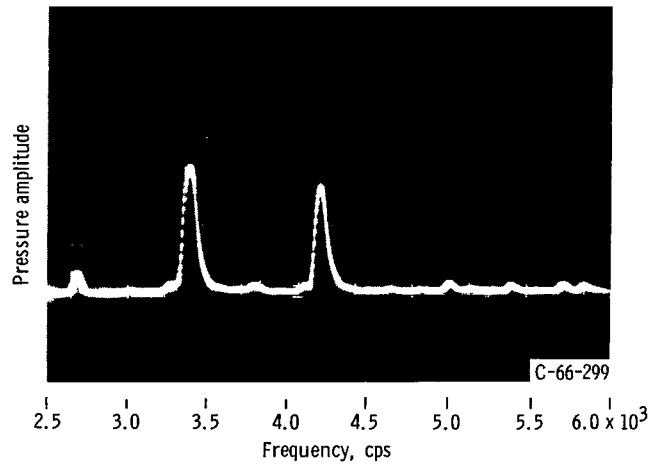


Figure 11. - Typical example of pressure oscillations during screech.

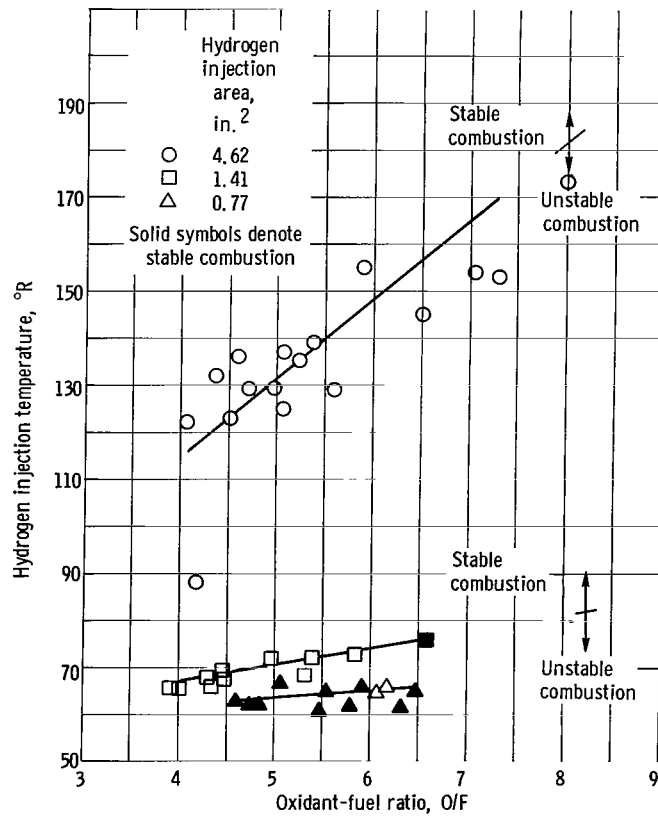


Figure 12. - Effect of hydrogen injection area on variation of screech transition temperature. Variation of hydrogen injection area at constant oxygen injection area of 0.089 square inch.

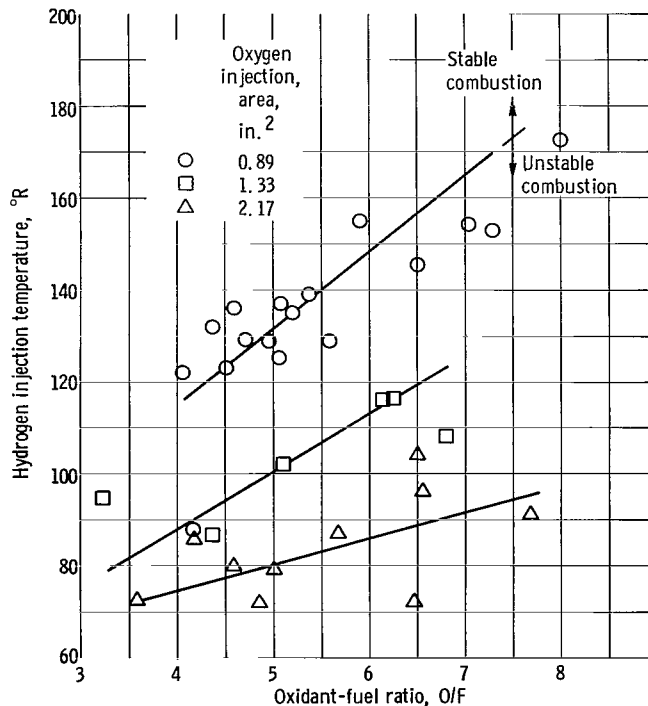


Figure 13. - Effect of oxygen injection area on variation of screech transition temperature. Variation of oxygen injection area at constant hydrogen injection area of 4.62 square inches.

responds to the frequency for the first transverse acoustic mode for the combustion chamber environment. The second pressure "spike" present appears to be a combined mode of first transverse and first longitudinal.

Effect of Propellant Injection Area

To determine the effect of hydrogen injection velocity on screech limits, the flow area of the hydrogen injection annuli was systematically varied while the oxygen injection area was held constant. Typical results are shown in figure 12 where the hydrogen temperature at the instant of screech transition is shown as a function of oxidant-fuel ratio. Each data point represents the result of a transient in hydrogen temperature such as those runs depicted in figure 10. Thus, the region above each curve represents a region of stable operation for that configuration, and, conversely, operation at hydrogen temperatures below the curve produces screech. It is seen that for each hydrogen injection area, the screech limit defined by the data is an approximately linear function of oxidant-fuel ratio. More important, however, is the very major improvement in the screech boundary that occurred when the hydrogen injection area was decreased. For the data shown at a constant oxygen injection area of 0.89 square inch and for operation at a mixture ratio of 5.0, the hydrogen temperature at which screech occurred was decreased

from 130° to less than 60° R. It should be noted that the solid symbols denote stable operation at the minimum hydrogen temperature available with the test installation.

Similarly, the effects of increasing the oxygen injection area (and, hence, reducing oxygen injection velocity) are shown by the data of figure 13 for a constant hydrogen injection area of 4.62 square inches. Again, the screech transition temperature increased linearly with increased oxidant-fuel ratio; however, the screech limits improved as the oxygen area was increased rather than decreased as was the case with hydrogen injection area variations. At an oxidant-fuel ratio of 5.0, the screech transition temperature was decreased from 130° to 80° R by an increase in oxygen injection area from 0.89 to 2.17 square inches.

The opposite effects of changing hydrogen injection area and oxygen injection area naturally suggests a phenomenon related to hydrogen-oxygen area ratio. Accordingly,

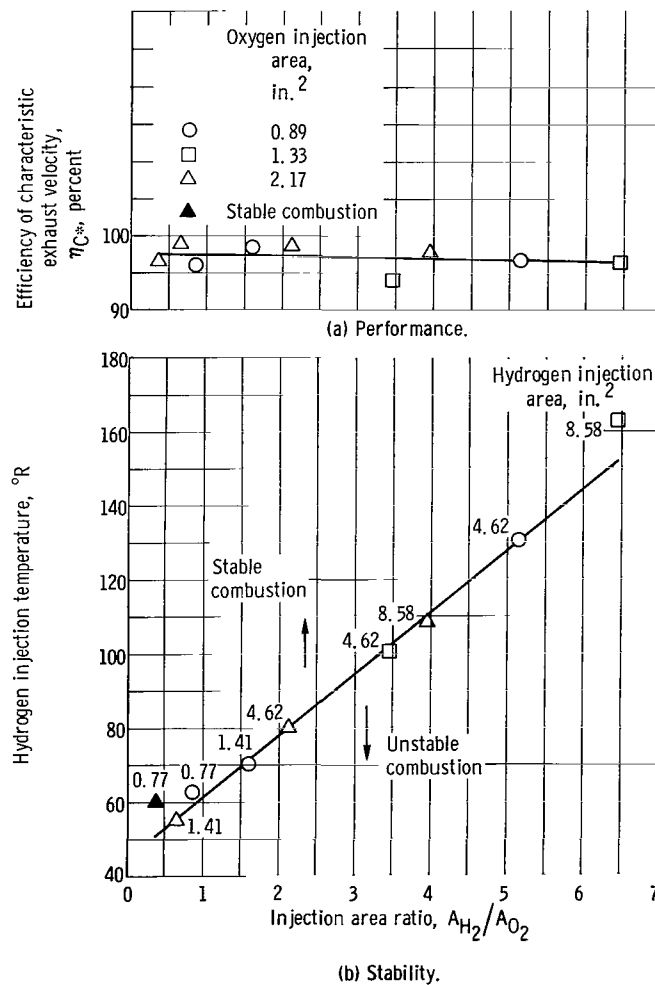


Figure 14. - Correlation of screech transition temperature with injection area ratio for conventional concentric tube element injectors. Oxidant-fuel ratio, 5.

the data of figures 12 and 13 along with similar data for all configurations listed in table I (except those with tapered or counterbored oxidizer tubes) were cross plotted at a mixture ratio of 5.0 (fig. 14). Hydrogen temperature at screech transition is plotted in figure 14(b) as a function of hydrogen-oxygen area ratio. Again, stable operation occurs at hydrogen temperatures above the curve, and screech occurs at hydrogen temperatures below the curve. It is seen that the screech limit improved linearly as the hydrogen-oxygen area ratio was decreased. Stable operation was obtained at hydrogen temperatures as low as 55° R although the minimum value at an area ratio of 0.36 could not be determined because of installation limitations.

The ability to operate at extremely low hydrogen temperatures without screech as the area ratio was reduced might be expected to result in a reduction in combustion efficiency. As shown by the data of figure 14(a), however, this was not the case. For these configurations employing 48 pounds of thrust per injector element, characteristic velocity efficiency remained nearly constant at $96\frac{1}{2}$ percent over the entire range covered.

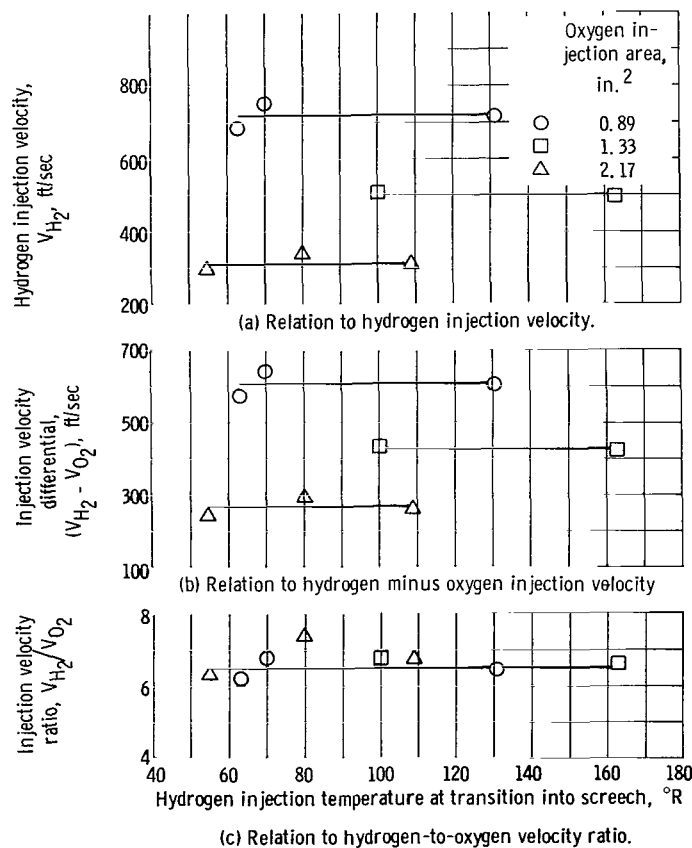


Figure 15. - Correlation of screech transition temperature with three injection velocity parameters. Oxidant-fuel ratio, 5.0.

Stability Correlation with Injection Velocities

In the previous figures, stability data have been correlated in terms of injection area ratio, a relation of direct use to an engine designer. The interplay between screech characteristics and injection velocities is, however, of more significance perhaps from a fundamental standpoint. Various investigators have hypothesized that screech characteristics may be associated with the propellant injection velocities, velocity or momentum ratio, or the differential velocity of the injected propellants. The relation of screech characteristics (minimum stable hydrogen temperature) to these terms is shown in figure 15 with the same data as was used in figure 14 at an oxidant-fuel ratio of 5.0. Screech occurred at widely different values of either hydrogen injection velocity (fig. 15(a)) or velocity differential (fig. 15(b)) for the three oxygen injection areas. In contrast, all of the data correlated reasonably well with the hydrogen-oxygen velocity ratio or momentum ratio since the oxidant-fuel ratio was constant (fig. 15(c)). The screech boundary occurred at a velocity ratio of about 6.5 for all configurations and over the entire range of hydrogen transition temperatures covered (165° to 55° R). Thus, injection velocity ratio is seen to be the determinant of screech boundary rather than hydrogen injection temperature as previously supposed. It is clearly indicated then that the effects of hydrogen temperature on screech occur as a result of the change in hydrogen density and the corresponding change in injection velocity ratio.

The previous velocity correlations were compared by using cross-plotted data because of the sensitivity of the velocity calculation to errors in temperature measurement. For example, an error of 3° R at a temperature of 70° R results in a 20 percent density change in hydrogen and, consequently, a corresponding error in velocity. Even with this extremely sensitive relation to temperature, a definite separation with oxygen injection areas was obtained when all the individual data points were correlated with either hydrogen injection velocity or injection velocity differential. The velocity ratio correlated all the individual velocity data fairly well for all injector configurations with about 75 percent of the data in a band between velocity ratios of $5\frac{1}{2}$ and $7\frac{1}{2}$.

The degree to which the correlation of screech boundary with hydrogen-oxygen velocity ratio established in figure 15 applies at mixture ratios other than 5.0 is shown in figures 16 and 17. These figures are identical with figures 12 and 13, except that curves for a constant velocity ratio have been superimposed. The close parallelism to the curves previously faired through the data and the small vertical displacement indicate that screech transition occurs at a velocity of about 6.5 for all data obtained at oxidant-fuel ratios between 4 and 7. Thus, the effect of oxidant-fuel ratio on screech limit appears to exist by virtue of the concomitant effect on injector velocity ratio. In figures 16 and 17, the velocity ratio lines are not equivalent to lines of constant momen-

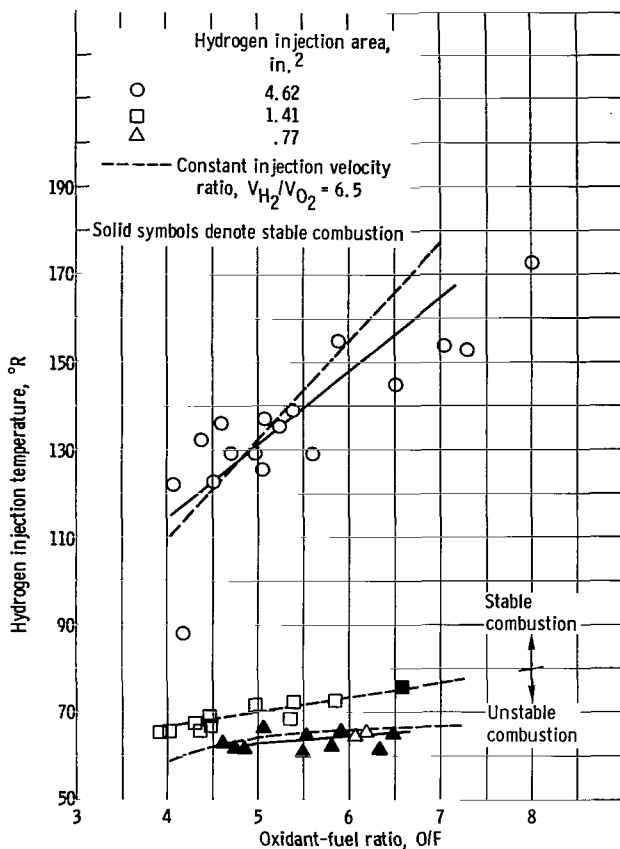


Figure 16. - Correlation of screech transition temperature with hydrogen-oxygen injection velocity ratio. Variation of hydrogen injection area at constant oxygen injection area of 0.89 square inch.

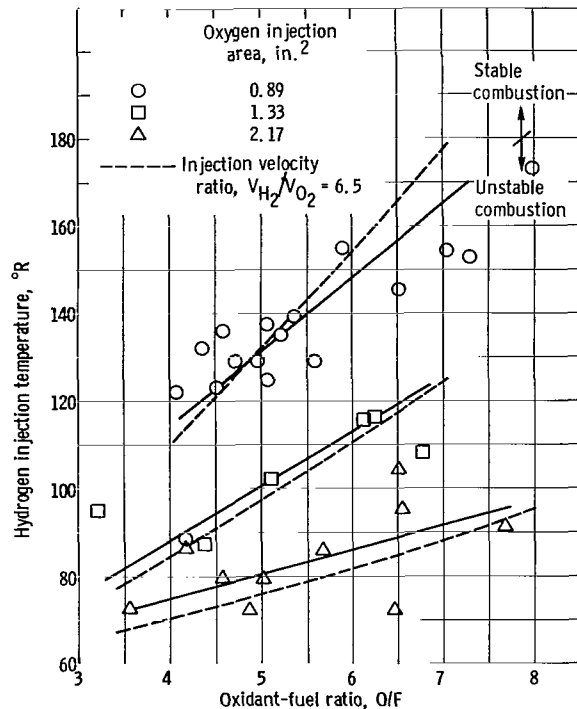


Figure 17. - Correlation of screech transition temperature with hydrogen-oxygen injection velocity ratio. Variation of oxygen injection area at constant hydrogen injection area of 4.62 square inches.

tum ratio since the oxidant-fuel ratio varies. The slope of the constant momentum ratio lines differed from the faired lines by approximately a factor of oxidant-fuel ratio.

Although velocity ratio seems to serve quite well as a correlating parameter, it is difficult to relate velocity ratio to a physical combustion model. Velocity ratio may, however, be symbolic of other more fundamental parameters. For example, since the oxidizer velocity V is related to the jet diameter squared D^2 , the velocity ratio could be converted by substitution to a numerically proportional parameter $V_{H_2} D_{O_2}^2$, which may be more meaningful with respect to a physical model.

The results of this investigation indicate that the designer can promote stability by utilizing velocity ratio through changes in either hydrogen temperature or injection area ratio. In regenerative engines, the designer usually has little if any chamber cooling margin. Accordingly, there is little latitude for the hydrogen temperature in the injector (cooling jacket outlet) to be increased as desired to obtain higher injection velocity ratios. Within certain constraints, however, the designer can achieve a wide range of values for

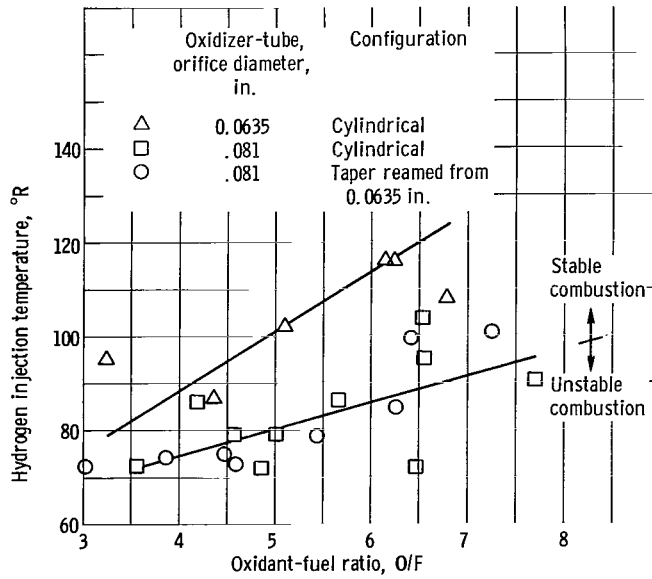


Figure 18. - Effect of oxidizer-tube taper on screech transition temperature. Hydrogen injection area, 4.62 square inches.

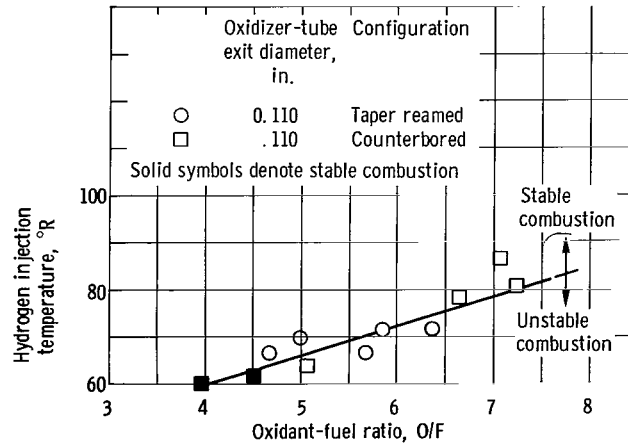


Figure 19. - Effect of oxidizer-tube taper and counterbore on variation of screech transition temperature. Hydrogen injection area, 4.62 square inches.

injector velocity ratios by changing injection area ratio. The constraints are (1) chugging that occurs generally at low values of oxygen pressure drop across the injector, (2) pump pressure limitations that may be encountered as hydrogen injection area is reduced in an effort to achieve higher values of injection velocity ratio, and (3) constraints on injection annuli imposed by machining or fabrication tolerances. To achieve such a high velocity ratio within these constraints, a designer could, however, take advantage of the techniques covered in the next section of this report.

Effect of Oxygen Tube Exit Geometry

Normally chugging is associated with low injector pressure drop, and the usual (but not always successful) solution is to increase the pressure drop until chugging disappears. On the other hand, the role of propellant injection hydraulics, in regard to screech, would be expected to be associated only with the exit conditions from the injector elements into the combustion chamber. It was therefore hypothesized that the constraints on pressure drop discussed previously could be relieved by combining a very large exit area on the oxidizer tubes to give the low oxidizer velocity needed for screech suppression with a relatively small bore in the entrance section of the tubes to maintain adequate pressure drop for chugging stability. The J-2 engine uses elements of this type.

Hydrogen temperatures for transition into screech are plotted in figure 18 as a function of mixture ratio for three oxidizer-tube configurations. Hydrogen injection area was constant at 4.62 square inches. When the diameter of the cylindrical bore was increased from 0.0635 to 0.081 inch throughout the length (fig. 6(a)) the screech limit improved significantly (40° R at a mixture ratio of 5.0). This was expected because of the reduced oxidizer velocity and consequent higher velocity ratio. Exactly the same result was obtained when tubes having a cylindrical bore diameter of 0.0635 inch were taper reamed at the exit to a diameter of 0.081 inch (fig. 6(b)). Thus, the screech characteristics appear to be related to the tube exit area. When the taper-reamed oxidizer tubes were further reamed out to an exit diameter of 0.110 inch (fig. 6(c)), a further improvement of about 15° R was found in the screech limit (fig. 19 as compared with fig. 18). It is noted also from figure 19 that the same beneficial effect was achieved by a cylindrical counter-bore (fig. 6(d)) to the same exit diameter.

The relation among screech limits for taper-reamed, counterbored, and straight-bore oxidizer tube configurations is illustrated in figure 20 in terms of the previously established correlation parameters of injection area ratio and velocity ratio. The solid curve for straight-bore oxidizer tubes is reproduced from figure 14. The dashed curve represents operation at a constant velocity ratio of 6.5 and is almost coincident with the solid correlation curve. Screech limits for both tapered and counterbored configurations

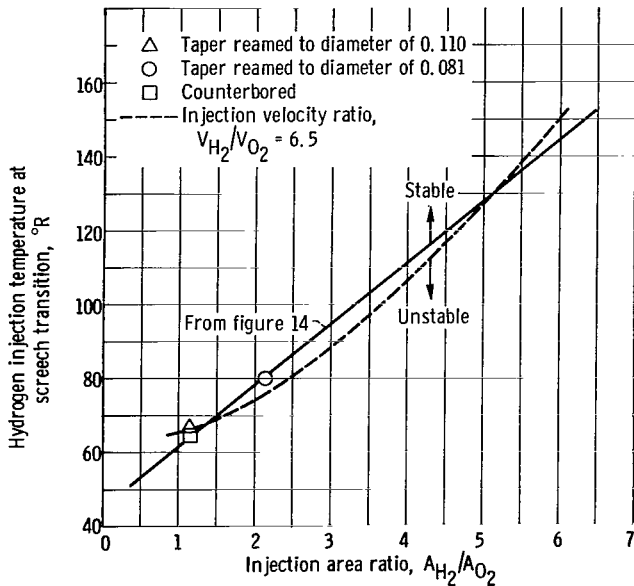


Figure 20. - Correlation of screech limits for tapered and counterbored oxidizer-tube configurations with area ratio and injection velocity ratio. Oxidant-fuel ratio, 5.0.

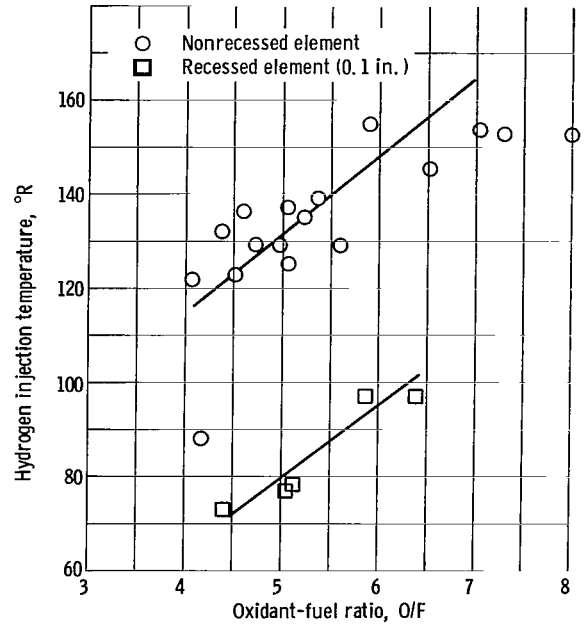


Figure 21. - Effect of oxidizer-tube recess on variation of screech transition temperature. Oxygen area, 0.89 square inch; hydrogen area, 4.84 square inches.

show excellent agreement with straight-bore configuration data when based on exit area ratio. The screech limit occurs at the same 6.5 velocity ratio shown earlier for the straight-bore configurations.

The effect on performance of taper reaming the oxygen tube exit from 0.0635 to 0.081 inch was insignificant as can be seen in table II; however, increasing the exit diameter to 0.110 inch produced a detrimental effect on combustion efficiency. The characteristic exhaust velocity efficiencies of counterbored and taper-reamed (0.110 in.) configurations were 3 and 5 percent lower than the straight-bore configurations.

In summary, from the data of figures 18 to 20, it appears that the use of taper or counterbore techniques will allow the large oxidizer tube exit area needed for screech suppression as well as maintain adequate injector pressure to avoid chugging instability.

Effect of Oxygen Tube Recess

While not related directly to the foregoing matrix of configurations used to delineate the effects of velocity ratio, one further configuration change is included as a matter of interest. In the J-2 engine development program, it was found that recessing the oxidizer tubes below the surface of the injector faceplate was beneficial in regard to both combustion stability and performance. Accordingly, the tubes of one injector configuration were recessed about 0.1 inch (fig. 6(e)). Comparative results are shown in figure 21.

For the recessed configuration, the hydrogen annulus (which tapers with axial station) was reduced so that the hydrogen injection area in the plane of the oxygen tube exit would be the same as the nonrecessed case. Examination of the data shows that the 0.1 inch recess improved the stability margin by about 50° R over the entire range of oxidant-fuel ratios. In view of this high degree of sensitivity to recess, one would expect that scatter in much of the experimental data might be associated with small inadvertent changes in recess produced by thermal distortion and machine tolerances. The reason for this marked effect of oxidizer tube recess on screech limit is not understood. In addition to improving stability, the recess also provided an increase in performance of about 3 percent.

SUMMARY OF RESULTS

An investigation was conducted to determine the effect of propellant injection velocity on screech in a 20 000-pound hydrogen-oxygen rocket engine. Stability data were obtained at a chamber pressure of 300 pounds per square inch absolute and a range of oxidant-fuel ratios from 4 to 7 for 13 concentric tube injectors. This investigation yielded the following results:

1. Screech boundary correlated with hydrogen-oxygen velocity ratio irrespective of hydrogen temperature. At velocity ratios above 6.5 operation was stable and below 6.5, unstable.
2. The hydrogen temperature at which screech occurred could be reduced to less than 60° R (minimum available) by selection of a hydrogen-oxygen injection area ratio of less than 1.0. Such selection results in a velocity ratio greater than 6.5 at very low hydrogen temperature (60° R).
3. Tapered or counterbored oxidizer tubes fit the correlation with velocity ratio based on tube exit dimensions; hence, this tube configuration may be used to keep high oxygen pressure drop for chugging stability margin.
4. Recessing the oxidizer tubes 0.10 inch below the surface of the faceplate improved stability in terms of screech transition temperature.

Lewis Research Center,
National Aeronautics and Space Administration,
Cleveland, Ohio, January 10, 1966.

APPENDIX A

SYMBOLS

A	measured injection area in plane of oxygen tube exit, in. ²	V_{H_2}	hydrogen injection velocity, ft/sec
A_{H_2}	hydrogen injection area, in. ²	V_{O_2}	oxygen injection velocity, ft/sec
A_{O_2}	oxygen injection area, in. ²	\dot{W}	propellant weight flow, ft/sec
A_t	area of throat, in. ² (determined from measurements taken prior to installation)	\dot{W}_{GH_2}	gaseous hydrogen weight flow, lb/sec
C_{exp}^*	experimental characteristic exhaust velocity	\dot{W}_{H_2}	hydrogen weight flow, lb/sec
C_{th}^*	theoretical characteristic exhaust velocity (ref. 4)	\dot{W}_{LH_2}	liquid hydrogen weight flow, lb/sec
g	gravitational conversion factor, (lb mass/lb force)(ft/sec ²)	\dot{W}_{O_2}	oxygen weight flow, lb/sec
I_1	theoretical specific impulse at inlet to nozzle, lb force-sec/lb mass (ref. 4)	\dot{W}_{STOR}	propellant mass accumulation in feed system
MPL	momentum pressure loss	ϵ	contraction ratio
P_c	total pressure in nozzle, psia	η_{C^*}	efficiency of characteristic exhaust velocity
P_{inj}	static pressure at injector, psia	ρ	propellant density, lb/ft ³ (determined from measured injection temperature and injector-face chamber pressure)
P_1	static pressure at inlet to nozzle, psi (derived from pressure ratio data of ref. 4)		
TWS	total weight stored		
V	injection velocity, ft/sec		
V_{avg}	average injection velocity, ft/sec		

APPENDIX B

METHODS OF CALCULATION

The measured hydrogen weight flow was corrected to account for the mass accumulation in the feed system caused by density change which occurred during the temperature ramped runs. A digital computer program, that had been developed for a heat transfer analysis to determine the hydrogen mass distribution in the cooling jacket of an engine was used to calculate the storage rate. The total volume of the feed system between the mixing station and the injector face which consisted of the mixer, torus, and injector cavity was considered in these calculations. A bulk density was determined at each report interval (0.032 sec) for each of three subvolumes from measured temperatures and pressures. The instantaneous total weight stored TWS was then determined by summing the products of density and volume of the three sections:

$$TWS_{t=i} = [\rho_1 V_1 + \rho_2 V_2 + \rho_3 V_3]_{t=i}$$

(Symbols are defined in appendix A.) The difference between TWS at $t=i$ and TWS at $t = i - 0.032$ second divided by the report interval of the sampled data (0.032 sec) represents the mass accumulation in the feed system \dot{W}_{STOR} . Thus, the instantaneous weight flow to the engine is found by:

$$\dot{W}_{H_2} = \dot{W}_{LH_2} + \dot{W}_{GH_2} - \dot{W}_{STOR}$$

The corrected hydrogen weight flow was used in calculations of combustion performance, oxidant-fuel ratio, and hydrogen velocity.

Efficiency of Characteristic Exhaust Velocity

Although the facility was equipped with an elaborate tripod-type thrust system, the measurements were not considered to be sufficiently accurate to present, thus characteristic exhaust velocity efficiency was used to compare the performance of the various injector designs. The following equations were used in calculating efficiency:

$$C_{exp}^* = \frac{P_c A_t g}{\dot{W}_T}$$

$$P_c = \frac{P_{inj}}{MPL}$$

$$MPL = \frac{P_1}{P_c} + \frac{I_1 \cdot g - V_{avg, inj}}{C_{th}^* \cdot \epsilon} \quad (\text{ref. 3})$$

$$V_{avg} = \frac{V_{H_2} \dot{W}_{H_2} + V_{O_2} \dot{W}_{O_2}}{\dot{W}_{O_2} + \dot{W}_{H_2}}$$

$$\eta_{C^*} = \frac{C_{exp}^*}{C_{th}^*}$$

Injection Velocity

The following equation was used in calculating the propellant injection velocities:

$$V = \frac{\dot{W}}{\rho A}$$

REFERENCES

1. Priem, Richard J. ; and Guentert, Donald C. : Combustion Instability Limits Determined by a Nonlinear Theory and a One-Dimensional Model. NASA TN D-1409, 1962.
2. Ladd, J. W. : A Durable and Reliable Test Stand System for High-Accuracy Temperature Measurements in the Cryogenic Ranges of Liquid Hydrogen and Liquid Oxygen. Vol. 6 of Advances in Cryogenic Engineering, K. D. Timmerhaus, ed., Plenum Press, 1961, pp. 388-395.
3. Huff, Vearl N. ; Fortini, Anthony; and Gordon, Sanford: Theoretical Performance of JP-4 Fuel and Liquid Oxygen as a Rocket Fuel. II - Equilibrium Composition. NACA RM E56023, 1956.
4. Gordon, Sanford; and McBride, Bonnie J. : Theoretical Performance of Liquid Hydrogen with Liquid Oxygen as a Rocket Propellant. NASA Memo 5-21-59E, 1959.

"The aeronautical and space activities of the United States shall be conducted so as to contribute . . . to the expansion of human knowledge of phenomena in the atmosphere and space. The Administration shall provide for the widest practicable and appropriate dissemination of information concerning its activities and the results thereof."

—NATIONAL AERONAUTICS AND SPACE ACT OF 1958

NASA SCIENTIFIC AND TECHNICAL PUBLICATIONS

TECHNICAL REPORTS: Scientific and technical information considered important, complete, and a lasting contribution to existing knowledge.

TECHNICAL NOTES: Information less broad in scope but nevertheless of importance as a contribution to existing knowledge.

TECHNICAL MEMORANDUMS: Information receiving limited distribution because of preliminary data, security classification, or other reasons.

CONTRACTOR REPORTS: Technical information generated in connection with a NASA contract or grant and released under NASA auspices.

TECHNICAL TRANSLATIONS: Information published in a foreign language considered to merit NASA distribution in English.

TECHNICAL REPRINTS: Information derived from NASA activities and initially published in the form of journal articles.

SPECIAL PUBLICATIONS: Information derived from or of value to NASA activities but not necessarily reporting the results of individual NASA-programmed scientific efforts. Publications include conference proceedings, monographs, data compilations, handbooks, sourcebooks, and special bibliographies.

Details on the availability of these publications may be obtained from:

SCIENTIFIC AND TECHNICAL INFORMATION DIVISION
NATIONAL AERONAUTICS AND SPACE ADMINISTRATION

Washington, D.C. 20546